Mitigating Medication Tampering and Diversion via Real-Time Intravenous Opioid Quantification

Tyler Hack, *Student Member, IEEE,* Joel Bisarra, *Student Member, IEEE,* Saeromi Chung, Shekher Kummari, and Drew A. Hall, *Senior Member, IEEE*

***Abstract*—Opioid tampering and diversion pose a serious problem for hospital patients with potentially life-threatening consequences. The ongoing opioid crisis has resulted in medications used for pain management and anesthesia, such as fentanyl and morphine, being stolen, substituted with a different substance, and abused. This work aims to mitigate tampering and diversion through analytical verification of the administered drug before it enters the patient. We present an electrochemical-based sensor and miniaturized wireless potentiostat that enable real-time intravenous (IV) monitoring of opioids, specifically fentanyl and morphine. The proposed system is connected to an IV drip system during surgery or post-operation recovery. Measurement results of two opioids are presented, including calibration curves and data on the sensor performance concerning pH, temperature, interference, reproducibility, and long-term stability. Finally, we demonstrate real-time fluidic measurements connected to a flow cell to simulate IV administration and a blind study classified using a machine-learning algorithm. The system achieves limits of detection (LODs) of 1.26 µg/mL and 2.75 µg/mL for fentanyl and morphine, respectively, while operating with >1-month battery lifetime due to an optimized ultra-low power 36 µA sleep mode.**

***Index Terms*—Fentanyl, morphine, potentiostat, wireless, opioid, electrochemistry.**

I. Introduction

OPIOIDS are an extremely effective class of analgesic drugs used for post-surgical pain management and relieving the symptoms of severe chronic illnesses [1], [2], [3]. Various types of opioids (*e.g.,* morphine, oxycodone, hydrocodone, tramadol, etc.) are prescribed in tablet/capsule form for at-home use or administered intravenously (IV) in a hospital setting, as shown in Fig. 1. Fentanyl is a particularly potent synthetic opioid (50–100× more potent than morphine) and is used as a surgical anesthetic [1]. The higher potency requires extreme caution, as even minor dosing errors can have a profound impact where a patient is at risk of residual pain if underdosed or addiction/dependency, respiratory depression, and death in the event of an overdose [3].

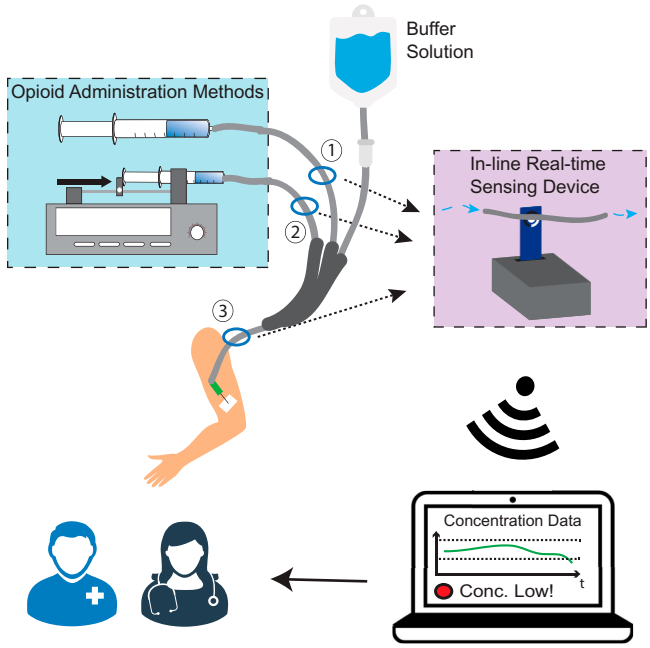

Fig. 1. Closing the loop of opioid administration by adding an opioid measurement device (1) after bolus dosage, (2) after continuous IV dosage, or (3) after dilution with buffer solution.

Unfortunately, the pain-relieving efficacy and euphoric effects experienced with opioids have led to a severe increase in addiction and overdose deaths over the past decade, resulting in a steadily worsening opioid epidemic. In 2021, the Centers for Disease Control and Prevention estimated that 220 people were dying from an opioid overdose every day in the U.S. [4]. These reports of opioid abuse/misuse frequently stem from instances where a highly potent drug, *e.g.,* fentanyl, is used as an adulterant in another illicit substance to enhance the effects, creating what is referred to as a "street drug."

However, the opioid crisis has progressed beyond the street drug market into hospitals. Numerous instances of opioid diversion and tampering have been recently reported [5], [6], [7], [8], [9], [10], [11]. These scenarios typically involve nurses or doctors stealing a patient's medication and substituting it with another substance, most commonly saline buffer, with the intent to satisfy their own dependency or divert the samples elsewhere for unlawful distribution [12], [13]. As a result, the affected

Manuscript received 15 February 2024; revised 18 April 2024; accepted 17 May 2024. Date of publication 30 May 2024; date of current version 13 August 2024. This work was supported by the National Institutes of Health (2R44DA044905). This paper was recommended by Associate Editor C.-C. Hung. *(Corresponding author: Drew A. Hall.)*

The authors are with the Department of Electrical and Computer Engineering, University of California, San Diego, La Jolla, CA 92093 USA (e-mail: drewhall@ucsd.edu).

Color versions of one or more figures in this article are available at https://doi.org/10.1109/TBCAS.2024.3405815.

Digital Object Identifier 10.1109/TBCAS.2024.3405815

patient received little or no pain medication during the surgical procedure. In one particularly alarming incident, the pain medication was substituted with tap water, a non-sterile fluid, leading to infections and the death of nine patients [14].

Hospitals try to prevent medication diversion and tampering through a multi-faceted approach predominantly focused on policy reform, employee education, and surveillance [12]. At the individual level, the drug administration pipeline starts with the pharmacist, who prepares/dilutes the drug samples to a stock concentration. From there, doctors or nurses further dilute the opioid to the prescribed dosage and meticulously verify that the correct volume and concentration is being prepared [15]. Finally, the opioid is administered to the patient, and their vital signs (*e.g.*, oxygen saturation, heart rate, and respiration rate) are closely monitored for adverse effects [1], [2], [16]. However, this entire procedure heavily relies on trust; no analytical verification was performed. Not all errors are intentional; non-malicious medication errors can also occur through pharmacokinetic miscalculations, faulty equipment, or miscommunication. Implementing a device to perform real-time detection and quantification of the opioid directly as it enters the patient would help "close the loop" by allowing doctors and nurses to rapidly respond to errors, mitigate potential harm, and ensure patients receive the correct dosage.

Opioids are administered intravenously during surgery via two methods: bolus dosage (quick delivery of the entire dose) and continuous infusion (slow administration over a prolonged time) [17]. A typical IV setup is illustrated in Fig. 1, highlighting that there are three potential locations where the opioid solution could be monitored: 1) directly in-line with the injection port (bolus dosage measurement), 2) after the infusion pump, or 3) downstream after further dilution with saline buffer. As such, adding an in-line sensing device could provide tremendous flexibility for regulating medication dosage.

This work reports an electrochemical measurement system for real-time monitoring of opioids, specifically fentanyl and morphine, to combat medication tampering and diversion. The hardware electronics are miniaturized, battery-operated, low-power (μW-level), and Bluetooth compatible. The opioid sensors provide sensitive target detection "out-of-the-box" and can be seamlessly attached to IV bag setups through the custom 3D-printed flow cell and packaging. This article expands upon the work presented in [18].

The remainder of this paper is organized as follows: Section II covers the opioid sensing principle, Section III describes the hardware, and Section IV explains the firmware implementation. Section V presents opioid detection measurements, and Section VI compares this work to prior work. Finally, Section VII presents concluding remarks.

II. Detection Principle

Opioids can be detected using a variety of methods, including liquid chromatography (LC) with mass spectrometry (MS) [19], [20], surface-enhanced Raman spectroscopy (SERS) [21], radioimmunoassay [22], and antibody-based biosensors [23]. Although these methods provide high sensitivity, they are often

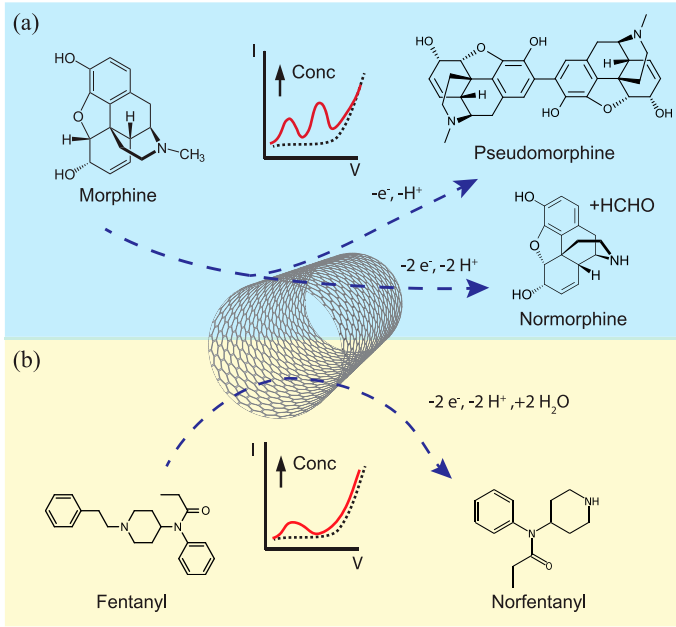

Fig. 2. Electrochemical detection principle illustrating the direct electrooxidation of (a) morphine and (b) fentanyl via a graphitic carbon WE.

expensive, confined to a centralized laboratory, and require trained personnel, making them unfavorable for the proposed real-time IV detection application. Electrochemical analysis offers a more promising avenue for clinical opioid monitoring due to its excellent sensitivity, rapid response time, and the required electronics can be miniaturized [24], [25], [26], [27].

Previous work has recently leveraged this to detect anesthetic drugs [28]. Among fentanyl sensors, electrodes modified with ionic liquids [29], [30], zinc-based metal-organic frameworks [31], and carbon nano-onions [32] have all shown promise for sensitive target detection. Similar detection schemes for morphine using carbon/graphene electrodes have also been reported [33], [34], alongside other modifications such as self-assembled monolayers [35], magnetic nanofibers [36], and enzymatic sensors [37]. These schemes all require modifying the electrode. Non-modified approaches were also reported where carbon inks [38], single-walled carbon nanotubes [39], and laser-carbonization [40] were utilized. Microneedle arrays [41] and microcatheter-based [42] opioid sensors have also been developed to continuously monitor patient response during surgery or postexposure. These *in-vivo* techniques are a tremendous advancement in real-time opioid monitoring, but as the opioid is not measured upstream prior to administration, they do not directly address tampering and diversion. Moreover, the aforementioned works focus solely on the electrochemical sensor; thus, the challenge of integrating these systems into pre-existing hospital IV setups remains unmet.

In this work, opioids are detected electrochemically via the principle of direct electrooxidation, where the oxidation of the target at its redox potential via the working electrode results in direct electron transfer. The potentiostat measures the subsequent electron loss, enabling compound identification. The electroactivity of morphine stems from its phenolic and tertiary amine groups. Illustrated in Fig. 2, oxidizing the phenolic ring

TABLE I
TARGET SPECIFICATIONS OF THE OPIOID MONITORING DEVICE

General Specifications		
Potential Sweep Range	0 – 1.2 V	
Potential Resolution	5 mV	
Solution Flow Rate	0.01 – 10 mL/min	
Battery Lifetime	≥ 1 day (scanning every minute)	
Sensor Specifications		
	Fentanyl	Morphine
Detection Range	5 – 50 [μg/mL] (bolus dosage)	10 – 100 [μg/mL] (post-mixing dosage)
Variability	< 10%	
Disposable?	Yes	

produces pseudomorphine and one electron, whereas oxidizing the tertiary group results in normorphine and two electrons. The corresponding voltammogram for morphine, therefore, contains two anodic peaks, one at +340 mV and another between +830–940 mV. Similarly, the fentanyl voltammogram displays a single distinct peak at +880 mV due to its oxidation into norfentanyl through an N-dealkylation reaction [38], [43]. Critically, these peaks' amplitude depends on the opioid concentration [33]. Thus, combining the peak current and potential position enables target quantification and discrimination. Direct electrooxidation is a simple, albeit non-specific, electrochemical technique to identify opioids that does not require a ligand (*e.g.*, aptamer) against an opioid [44], [45].

A graphitic carbon working electrode is required to catalyze the opioid oxidation reaction [46]. This was achieved by employing a screen-printed electrode (SPE) from DropSens (SPE-150), which has a carbon working electrode (WE), a platinum counter electrode (CE), and a silver reference electrode (RE). Selecting this type of SPE for this application provides several advantages over conventional solid-metal electrodes and home-made SPEs. Specifically, they provide 1) a reduction in cost for the overall system, 2) easy disposability post-use to prevent cross-contamination, and 3) they are already mass-produced. Differential pulse voltammetry (DPV) was utilized to readout the sensors since it partially cancels the capacitive electrode background currents, enabling highly sensitive detection of low-level analytes and enhanced peak voltage resolution compared to more straightforward methods like chronoamperometry and cyclic voltammetry [47]. Ultimately, the proposed sensing scheme offers sensitive and rapid detection of both fentanyl and morphine with a single commercially available sensor that requires no additional modification or pre-treatment steps, rendering this a favorable solution for hospital integration. Table I summarizes the opioid monitor design requirements.

III. HARDWARE DESIGN AND OPTIMIZATION

The opioid monitoring device was designed to support seamless integration into pre-existing hospital IV bag systems by eliminating its dependency on complex or bulky instrumentation. To accomplish this, the reported system is: 1) fully wireless to provide remote control and data transmission to a nearby computer for visualization and post-processing; 2) battery-powered and rechargeable with ultra-low power consumption to maximize operation lifetime; and 3) miniaturized to enhance portability. Importantly, achieving these goals does not come at the cost of device performance and measurement sensitivity, as will be shown later. The opioid monitor consists of a flow cell that houses the SPE sensor and a custom-designed potentiostat that performs the electrochemical measurements with wireless data telemetry, enabling doctors or nurses to analyze the collected data and respond accordingly.

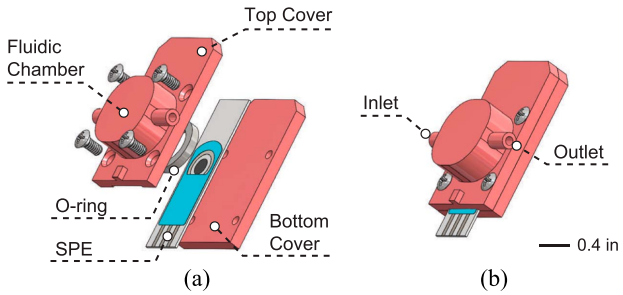

Fig. 3. 3D-printed flow cell model renderings of the (a) exploded and (b) assembled views. The screen-printed electrode is housed within the flow cell.

A. Flow Cell

Measuring the opioid solution as it travels through IV tubing requires a constant flow rate and volume. This is achieved through a 3D-printed flow cell placed between the patient and the opioid injection port by connecting it in line with standard IV tubing. The custom-designed flow cell (see Fig. 3) guides the solution into a fluidic chamber housing the SPE. The flow cell consists of two parts, labeled Top Cover and Bottom Cover, which sandwich the SPE together via screws. An O-ring is utilized for sealing. The 80 μL flow cell was designed using SOLIDWORKS and printed on a resin-based 3D printer (FormLabs 3B). To avoid biocompatibility concerns with this system, the parts can be printed with a biomedical grade resin (RS-F2-BMBL-01, FormLabs) certified for pharmaceutical and drug delivery applications.

B. Device Assembly

An annotated image of the assembled printed circuit board (PCB) is provided in Fig. 4(a). Including all connectors, the device occupies an area of only 2.73 in^2. The battery is located underneath the PCB, which is housed within a 3D-printed enclosure [Fig. 4(b)] to prevent fluidic leakage onto the circuitry. The flow cell plugs directly into the SPE connector, allowing the entire device to hang from an IV setup.

C. Potentiostat Signal Path

A block diagram of the reported device is shown in Fig. 5, illustrating the potentiostat, microcontroller/radio, and associated power management. The potentiostat is implemented with the Analog Devices AD5940 analog front-end, as it provides a fully integrated solution with a wide range of reconfigurability and

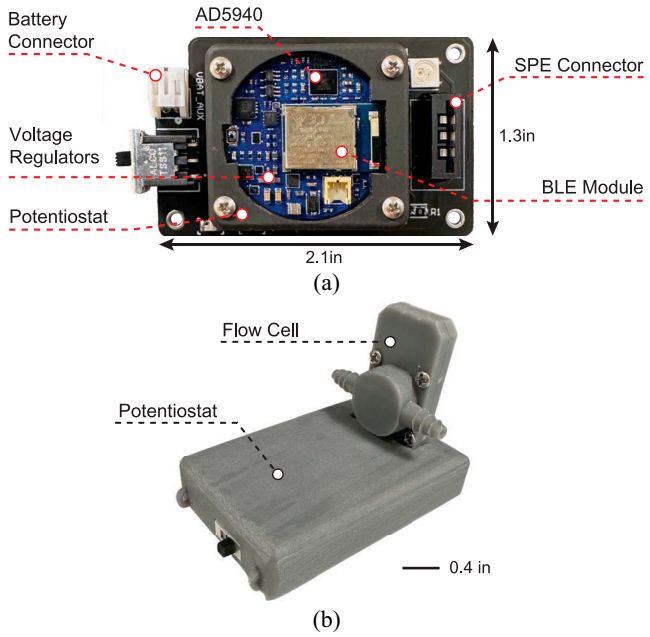

Fig. 4. Annotated photographs of the hardware showing the (a) potentiostat circuit board and (b) fully assembled device inside the 3D-printed case.

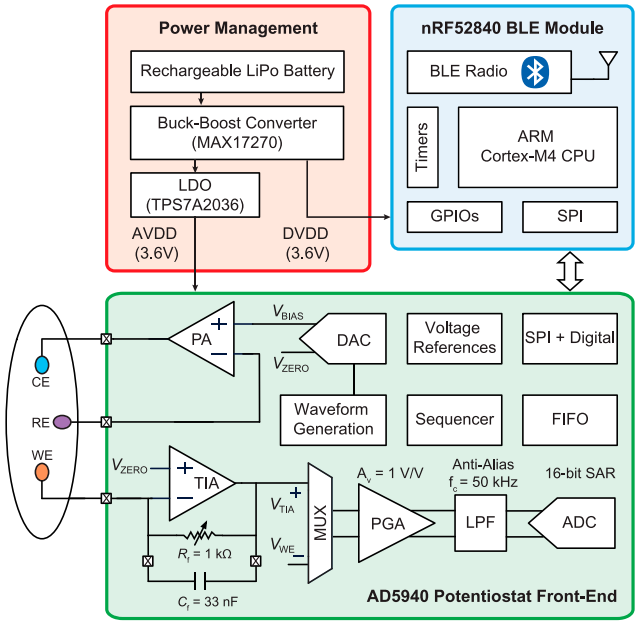

Fig. 5. Detailed block diagram of the opioid monitoring system electronics.

low power consumption. By integrating the front-end amplifiers, digital-to-analog converters (DACs), analog-to-digital converter (ADC), and digital back-end into a single chip, the overall PCB area can be considerably reduced compared to prior-art discrete potentiostats [25], [26], [48], [49]. The AFE interfaces with the 3-electrode electrochemical cell via a 3-pin edge connector.

DPV waveform generation is accomplished through the dual-output DAC, timers, and on-chip sequencer, which allows pre-programmed measurement procedures to be loaded into the AD5940 for autonomous execution. After configuration with the desired parameters, the DAC outputs the superimposed square and staircase waveform through its two outputs, V_{BIAS} and V_{ZERO}. The V_{BIAS} output has a 12-bit resolution (537.2 µV step size), while the V_{ZERO} output only has a 6-bit resolution (34.38 mV step size). As such, the V_{ZERO} voltage is held constant during a scan, while the V_{BIAS} is modulated due to its superior resolution. Both DAC outputs can be independently configured between 0.2 and 2.4 V, enabling a potential sweep range of $>$1.2 V. As a result, the 12-bit output satisfies the potential requirements from Table I.

This waveform is applied to the electrochemical cell via a potentiostat amplifier (PA) and transimpedance amplifier (TIA), which operate in negative feedback to maintain the RE and WE potentials (V_{RE} and V_{WE}) at V_{BIAS} and V_{ZERO}, respectively. The TIA converts the sensor redox current into a voltage, the output of which is sent to the positive input of a low leakage MUX alongside V_{WE} to the negative input. Alternatively, the negative MUX input can measure the direct DAC output (V_{ZERO}) instead. It was verified that the MUX leakage is sufficiently low to introduce negligible error on the final current measurement. The TIA gain is programmable on-chip via resistor R_{f}, which was set to 1 kΩ for all measurements. An off-chip 33 nF capacitor, C_{f}, ensures TIA stability in the presence of the large double-layer capacitance. This *RC* feedback network realizes a low pass filter (LPF) with a cutoff frequency of 4.82 kHz, suppressing noise without limiting the settling time of the TIA due to the pulsed DPV transients.

The remainder of the signal path conditions the differential signal (V_{TIA}–V_{WE}) before digitization. A programmable gain amplifier (PGA) and anti-aliasing filter (AAF) ensure the signal sits within the ADC input range while further rejecting high-frequency noise. The PGA gain was set to 1 V/V, and the AAF was configured to its minimum setting (50 kHz) since the TIA already limits the signal bandwidth to 4.82 kHz. Finally, the signal is sampled and digitized by a 16-bit ADC.

D. Microcontroller and Radio

A Nordic nRF52840 Bluetooth Low Energy (BLE) System-on-Chip (SoC) was selected to control the AFE operation, collect the measured data, and transmit the data wirelessly. The SoC is packaged within the MDBT50Q module from Raytac and integrates an ARM Cortex-M4 microcontroller (MCU), BLE radio, and chip antenna. This SoC was chosen for its low-power operation in sleep modes and wide range of necessary peripheral functions, including an ADC, timers, serial peripheral interface (SPI) communication, and general-purpose I/O (GPIO) pins. When communicating over BLE, the radio consumes only ~6.4 mA during transmission, and the entire SoC can be placed into a low-power sleep state ($<$10 µA) when a measurement is not being performed or when the MCU is idle and waiting for new data. These features have been leveraged to significantly extend the battery lifetime of the system.

E. Power Management

A 500 mAh rechargeable Lithium-Ion Polymer (LiPo) battery (LP503035) was selected to power the system with a nominal

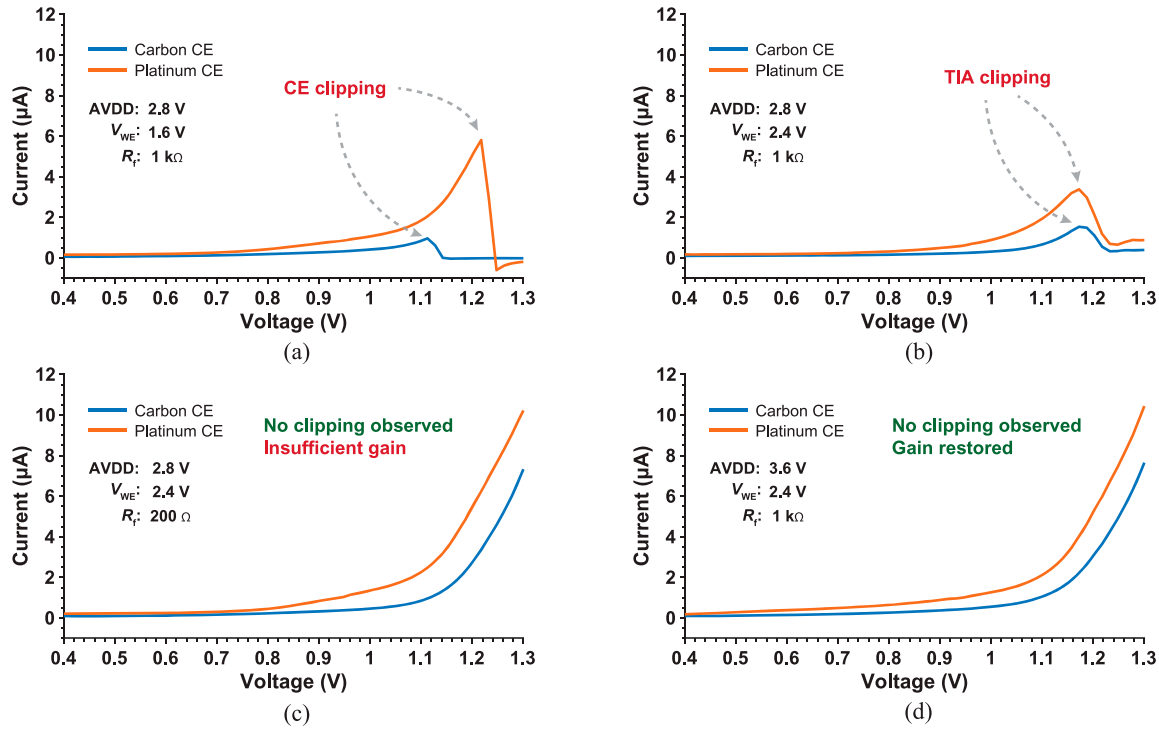

Fig. 6. Sequence of optimizations to prevent CE and TIA clipping inside the potentiostat. Voltammograms in 1× PBS comparing responses of a carbon and platinum CE with different AFE configurations: (a) minimum supply voltage, midscale V_{WE}, and desired TIA gain; (b) minimum supply voltage, maximum V_{WE}, and desired TIA gain; (c) minimum supply voltage, maximum V_{WE}, and reduced TIA gain; (d) maximum supply voltage, maximum V_{WE}, and desired TIA gain.

voltage of 3.7 V and a usable range of 3.0 to 4.2 V. Given the desire to operate the AD5940 at its maximum supply voltage of 3.6 V (for reasons that will be clear later), this necessitates utilizing a buck-boost converter. However, the output voltage ripple associated with switching regulators can impact the measurement fidelity of the AD5940. Placing a low-dropout regulator (LDO) after the buck-boost converter solves this problem. The MAX17270 buck-boost converter was selected for its high efficiency and sub-µA quiescent current. It generates a 4.1 V output to give some dropout before feeding into the TPS7A2036 LDO, which generates the low-noise, ripple-free 3.6 V supply (AVDD) for the AD5940. Although this scheme of boosting the battery voltage and then down-regulating via the LDO has a power penalty, it is necessary to achieve the required potentiostat compliance voltage while removing the supply ripple. Conveniently, this buck-boost converter features multiple output channels, allowing the MCU to be powered off a separate rail (DVDD) also at 3.6 V to prevent digital switching transients from coupling into the analog circuitry. This split rail setup also allows the LDO (and AFE) to be power gated when not used, reducing the system's quiescent power and the extra power overhead associated with the LDO conversion.

F. Counter Electrode and AFE Optimizations

Due to the large oxidation potentials of fentanyl and morphine (∼900 mV), a wide potential scan range is required to fully resolve the peaks of these opioids. A minimum upper bound of the potential range is 1.2 V, which poses several challenges for the potentiostat and is difficult to implement in a low-power battery-operated system. Namely, the potentiostat's compliance voltage, defined as the maximum achievable potential difference between the WE and CE, must be significantly greater than 1.2 V to provide enough headroom for the CE overpotential and avoid either of the amplifiers in the potentiostat from clipping.

Referring to the front-end schematic in Fig. 5 and considering the node potentials at the end of a DPV scan up to 1.2 V, it is clear that a 1.2 V potential difference will exist between the WE and RE. The electrochemical cell can be modeled with a Randles circuit; thus, the CE will have an even lower potential than the RE. However, the magnitude of this extra difference is variable and heavily dependent on the CE material, analyte concentration, and DPV parameters. If, at any moment, the CE reaches the lower bound on the PA's output range, the potentiostat loop will be disrupted, introducing a hard nonlinearity/clipping to the measurement.

There are three knobs available to the designer that should be optimized to mitigate CE clipping. The first is the WE voltage (with respect to GND), the second is the choice of AFE supply voltage, and the third is the CE material. Recall that using a carbon WE is necessary for the opioid sensing principle in this work, but the CE does not have such a restriction. The CE clipping behavior was studied to evaluate this, and the DPV parameters were optimized. The results of this study are presented in Fig. 6 under different WE potential, AFE supply voltage, and TIA gain settings. Each panel displays the voltammogram from a DPV scan of 1× phosphate buffer saline (PBS) solution up to 1.3 V for a carbon CE (SPE-C110) and a platinum CE (SPE-150). During all measurements, the time domain responses of

the CE and TIA output nodes were probed with an oscilloscope. In Fig. 6(a), the TIA gain is 1 kΩ, the AFE supply voltage is set to the minimum of 2.8 V, and V_{WE} is set to a moderate value of 1.6 V, leaving 400 mV of headroom for the CE when the scan reaches 1.2 V. The voltammograms show that the carbon CE clips at 1.11 V, whereas the platinum CE reaches 1.21 V before clipping, demonstrating a ∼100 mV lower overpotential than carbon. Probing the CE for each electrode type during the scan also confirmed this, as both nodes were observed to flatline at 0 V before the end of the scan.

In Fig. 6(b), the TIA gain and AFE supply voltage are unchanged, while V_{WE} is increased to its max value of 2.4 V (increasing the CE headroom to 1.2 V). This time, however, both electrodes clipped at 1.17 V, but the source of the clipping was observed to move from the CE to the TIA output, now clamping at 2.8 V. Given that the available TIA output swing is bounded on the high side by the 2.8 V supply voltage, increasing the WE potential further limits this range. A simple modification to this configuration is to reduce the TIA gain, shown in Fig. 6(c), to 200 Ω. By doing this, no clipping was observed with either electrode across the entirety of the scan. However, being forced to reduce the gain results in a 14 dB loss in front-end sensitivity, rendering this approach a non-ideal solution. Fig. 6(d) presents a better approach, which leverages the final design variable, the AFE supply voltage, to mitigate CE and TIA clipping simultaneously without sacrificing measurement sensitivity. V_{WE} is kept at 2.4 V, the TIA gain is returned to 1 kΩ, and the AFE supply voltage is raised to the maximum, 3.6 V. Once again, no clipping was observed with either amplifier. Despite this approach requiring a larger voltage (thereby increasing the power consumption of the system), it is a necessary tradeoff to achieve such a large compliance voltage without hindering the achievable opioid sensitivity. These experiments also demonstrate the importance of selecting a CE material that minimizes the overpotential. Although Fig. 6(d) suggests that either material could suffice, the overpotential will increase further with the target analyte added to the solution. As such, the platinum CE was selected for this work to ensure that this does not occur across the targeted range of fentanyl and morphine.

IV. Firmware Operation

The MCU configures the AD5940 with the desired AFE settings and DPV parameters, collects data during a scan, and maintains the BLE connection. However, careful construction of the firmware operation and BLE protocol plays a significant role in reducing the average power consumption of the device. A firmware flow chart is presented in Fig. 7.

After power-up, the MCU undergoes hardware initialization and begins advertising for central BLE devices. Once a central device establishes a connection, the MCU immediately enters a deep sleep to minimize its idle current draw. The MCU also powers down the potentiostat (via the LDO) in this state to reduce power consumption further. While asleep, all subsequent functionality is handled via individual interrupt service routines (ISRs), such that the MCU can return to its sleep state after executing a given task. A total of four ISRs are used to implement

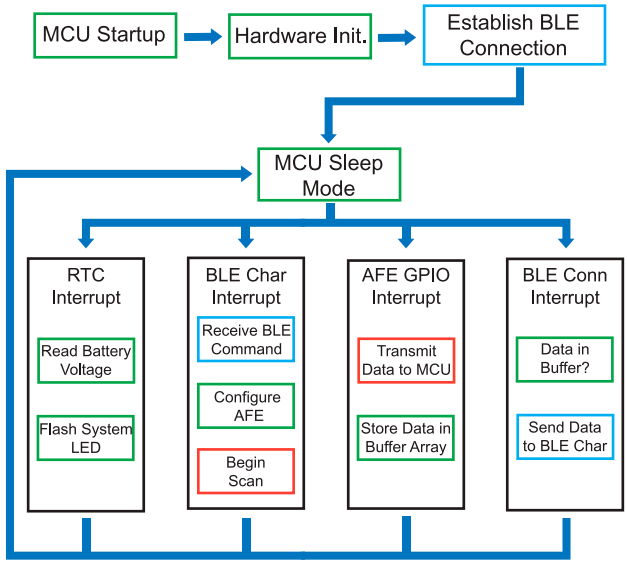

Fig. 7. Device firmware flow diagram illustrating the sleep mode and event-driven operation through dedicated interrupt routines.

the required functionality. The first is a simple timer-based interrupt used for housekeeping tasks, including flashing a light-emitting diode (LED) as a status indicator and recording the battery voltage level with the MCU's built-in ADC to assess whether a recharge is required.

The second ISR occurs when the central device updates the required AFE settings or measurement parameters stored within a dedicated BLE command characteristic. This information contains parameters such as the scan range, scan rate, current range, etc., or start/stop commands used for measurement execution. After updating the characteristics, the MCU reconfigures the AFE as needed.

Two final ISRs handle data transmission and reception between the AD5940 and MCU over SPI or between the peripheral and central devices over BLE. Due to the on-chip sequencer inside the AD5940, measurements are executed autonomously after the MCU initializes a scan. Voltage and current data are collected by the AFE and stored in its internal FIFO. Once the buffer is full, the AD5940 triggers a GPIO interrupt within the MCU, allowing the data to be acquired over the SPI bus. Importantly, the MCU remains asleep between these GPIO interrupts to save power. Due to the slow scan times and low data rates associated with DPV (each scan takes ∼26 s and collects only 32 kB of data), adopting BLE over the more traditional Bluetooth classic achieves substantial power savings. Rather than keeping the transmitter or receiver always on and listening, the infrequent nature of the interrupts allows the BLE radio to remain off for most of the scan. Instead, the radio is only active during periodic connection intervals (acting as the fourth ISR), which occur at a fixed period (100 ms in this work) and allow the MCU to check if new data has been collected. If received, the new data is transmitted to the central; otherwise, the MCU and radio return to sleep.

This interrupt-based firmware operation significantly reduces the average power consumption of the overall device. Combined

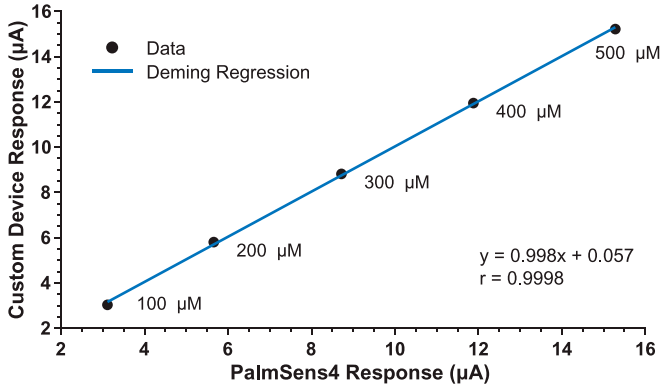

Fig. 8. Electrochemical benchmarking of the custom reported potentiostat vs. a commercial PalmSens4 device. Deming regression fit comparing measured results of DPV scans in potassium ferri-/ferro-cyanide.

with carefully selecting low-power integrated circuits, the system consumes only 36 µA during sleep mode and 12.3 mA during electrochemical measurements. The battery lifetime can then be calculated as a function of how frequently DPV scans are performed. For example, for a 500 mAh battery capacity and a 26-second scan time, running a DPV scan once per minute results in an average current draw of 5.35 mA and a 3.9-day battery lifetime. If the sampling rate is reduced to 10 minutes, the average current drops to 567 µA, extending the operating lifetime to 36.75 days. These measurements were taken directly at the battery input using a precision source measure unit (Keithley 2604B) and accounted for all components on the PCB. This 1-month device lifetime refers strictly to the battery's lifetime before a recharge is needed. The lifetime of the electrochemical sensors will be discussed separately in Section V. Regardless of the opioid administration method, whether it be a quick bolus dosage during surgery or a prolonged self-administration for pain relief, battery lifetime will not hinder operation.

V. Measurement Results

A. Reagents and Instrumentation

Fentanyl (#F-013-1ML), morphine (#M-005-1ML), phosphate buffer saline (#P5493), ascorbic acid (#A2218), uric acid (#U2625), glucose (#G7528), sucrose (#S7903), and fructose (#F0127) were obtained from Sigma-Aldrich. Acetaminophen (#A11240) and caffeine (#39214) were purchased from Alfa Aesar, Inc. All other chemicals were analytical grade reagents (>99% purity). Buffer pH adjustments were made using 100 mM hydrochloric acid (for acidic pH) or 100 mM sodium hydroxide pellets (for alkaline pH) and validated with a pH meter (Orion Star A211). Temperature measurements were performed in a temperature-controlled water bath (PolyScience #WBE02A11B).

Fentanyl[1] is distributed to hospitals in 50 µg/mL stock concentrations and can be further diluted as low as 5 µg/mL before administration, depending on an individual patient's weight and age [50]. Morphine, on the other hand, is distributed at 1 mg/mL and can be diluted down to 0.1 mg/mL before administration [51]. The reference standards for these controlled substances are sold in 1 mg/mL ampules containing only 1 mL (diluted in methanol). Both opioids were further diluted prior to measurement to conserve reagents and dilute the methanol. By doing so, the upcoming fentanyl measurements are representative of sensing location (1) from Fig. 1, while the morphine data corresponds to position (3).

[1]**Safety note:** Fentanyl is potentially lethal, even as little as 0.25 mg [52]. All experiments involving fentanyl were conducted inside a fume hood, wearing personal protective equipment per a university-approved handling protocol.

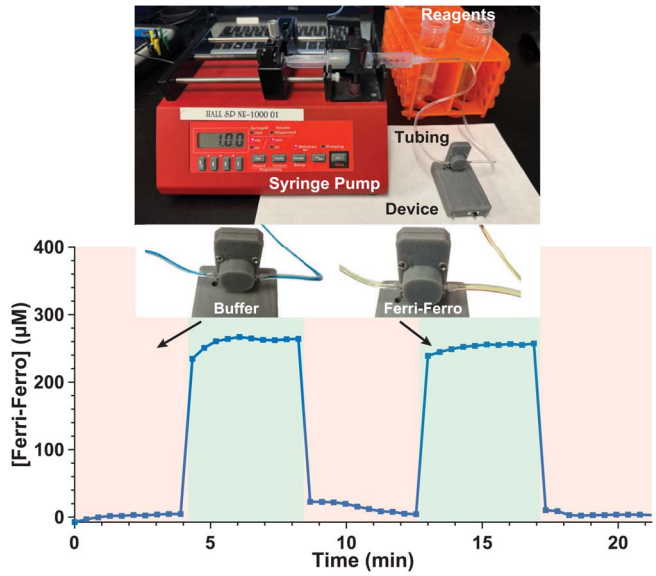

Fig. 9. Real-time consecutive DPV measurements with the flow cell connected to a syringe pump with alternating 1× PBS and potassium ferri-/ferro-cyanide solutions. Insets show photographs of the measurement setup and flow cell at various time points.

A 4 mm diameter carbon WE, platinum CE, and a silver RE screen-printed electrode from Metrohm DropSens (SPE-150) was used for all the electrochemical measurements. Unless stated otherwise, all concentrations were diluted in 1× PBS (pH 7.4). DPV measurements were performed using the custom reported potentiostat or a PalmSens4 (for comparison) with the parameters: 0–1.2 V scan range, 10.2 mV step voltage, 25 mV pulse, 50 ms pulse, and a 51 mV/s scan rate. Post-processing and statistical analysis of data was performed in MATLAB. All data displayed with error bars were obtained from three independent experiments with different sensors. Error bars represent one standard deviation.

B. Benchmarking With a Commercial Potentiostat

Before performing opioid experiments, the performance of the custom potentiostat was benchmarked against a commercial potentiostat (PalmSens4). DPV measurements were performed on solutions containing an equal parts mixture of potassium ferri-/ferro-cyanide ($K_3[Fe(CN)_6]$)/($K_4[Fe(CN)_6]$) diluted in 1× PBS with concentrations ranging from 100 – 500 µM. Fig. 8 compares the two potentiostat responses alongside a Deming regression fit. The response possesses a slope and Pearson correlation coefficient extremely close to unity, demonstrating a near-perfect equivalence between the two potentiostats.

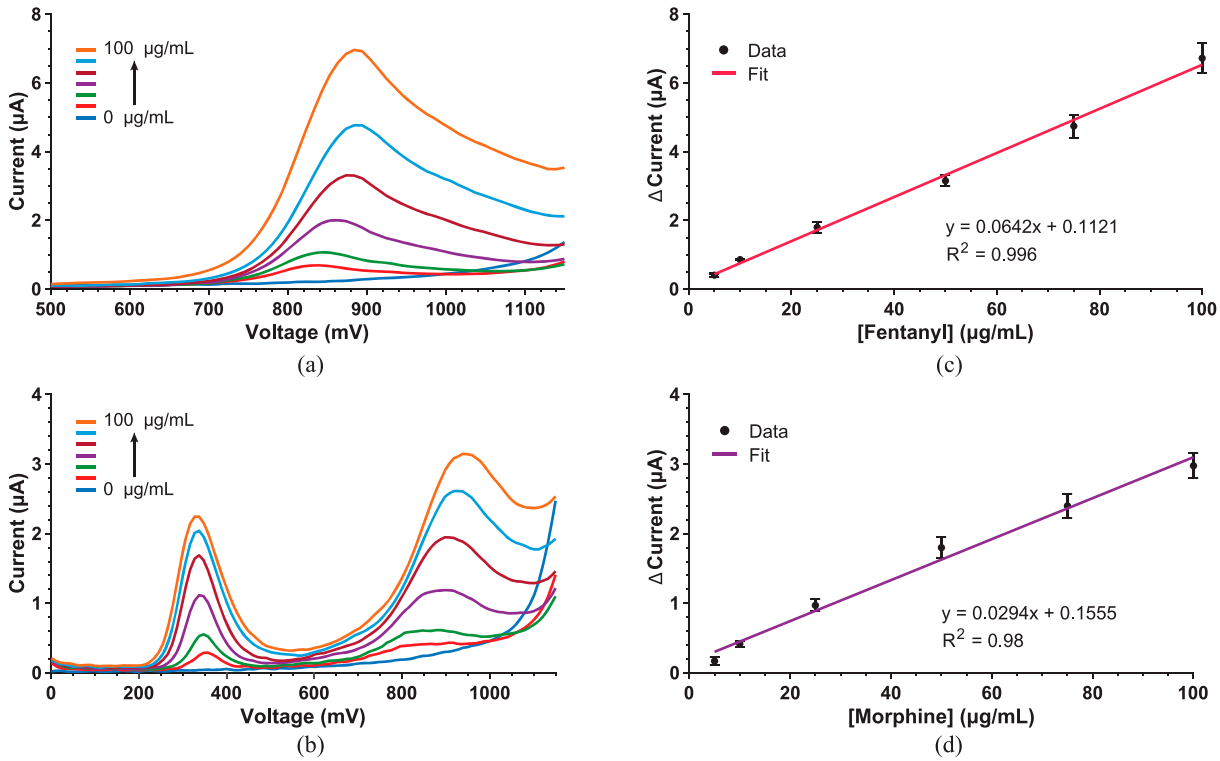

Fig. 10. Electrochemical opioid sensor characterization in 1× PBS (pH 7.4). Measured voltammograms across the therapeutic range for (a) fentanyl and (b) morphine with corresponding calibration curves ($n = 3$) presented in (c) and (d), respectively. Concentrations measured at 5, 10, 25, 50, 75, and 100 µg/mL.

C. Flow Cell Testing

The flow cell was installed onto an SPE sensor and connected to a syringe pump via tubing to validate the device in a scenario that emulates the clinical use case. Dynamic fluid measurements were then taken at a 1 mL/min flow rate every 26 seconds (continuous and consecutive DPV scans). The measurement setup and results are depicted in Fig. 9, where independent solutions containing 1× PBS and 250 µM ferri-ferro (diluted in 1× PBS) were alternately flowed through the cell and SPE sensor. The PBS solution was dyed blue for contrast to highlight the switching of the fluids. The corresponding ferri-ferro voltammogram peaks were extracted, converted back into a concentration using a previously generated calibration curve for ferri-ferro, and plotted as a function of time. The data demonstrates a strong "square-wave-like" pattern and accurate quantification of the analyte solution, which allows the target analyte to be clearly distinguished from saline as they alternate through the flow cell. Note that the transient signal after the buffer solution is switched back in is due to carry-over mixing and flushing of the flow cell that gradually decays over successive scans. These results validate the flow cell's functionality and the system's ability to accurately conduct fluid measurements. Although this is a simulated setup, it closely mimics how intravenous opioids are administered clinically. Since the solution is sensed prior to injection in a patient, the lack of patients in this study makes no difference to the measured data.

D. Electrochemical Detection of Fentanyl and Morphine

The electrooxidation response for fentanyl and morphine was investigated over the concentration range from 5 to 100 µg/mL. The resulting voltammograms are shown in Fig. 10. A well-defined electrooxidation peak was observed at ∼880 mV for fentanyl and two peaks for morphine, the first at ∼340 mV and the second at ∼830–940 mV. The oxidation peak currents increased linearly with concentration. For morphine, the second peak was found to have higher sensitivity and linearity than the first peak. As such, the calibration curve (and all subsequent morphine data) is plotted using the second peak current. The calibration curves demonstrate strong linear relationships with a regression coefficient of 0.996 for fentanyl and 0.98 for morphine, as shown in Fig. 10(c) and 10(d), respectively. The fentanyl sensor exhibited a sensitivity of 64.2 nA/(µg/mL) and a limit of detection (LOD) of 1.26 µg/mL, whereas the morphine sensitivity was 29.4 nA/(µg/mL) with an LOD of 2.75 µg/mL. The LOD was computed as three times the blank sample's standard deviation divided by the calibration curve's slope [53].

Due to the electrooxidation scheme, some of the opioid molecules are consumed by the reaction, slightly reducing the concentration and generating byproducts (norfentanyl, normorphine, and/or pseudomorphine) that will be injected into the patient. It was calculated that only 0.29% of fentanyl molecules and 0.17% of morphine molecules were consumed during the measurement. As such, the drug concentrations remain $>$ 99.7% and 99.8% of their original values for fentanyl and morphine, respectively, resulting in a negligible impact on the delivered concentration. The byproducts are all inactive metabolites, meaning they are nontoxic and pharmacologically inactive, presenting no safety concerns to the patient [54], [55].

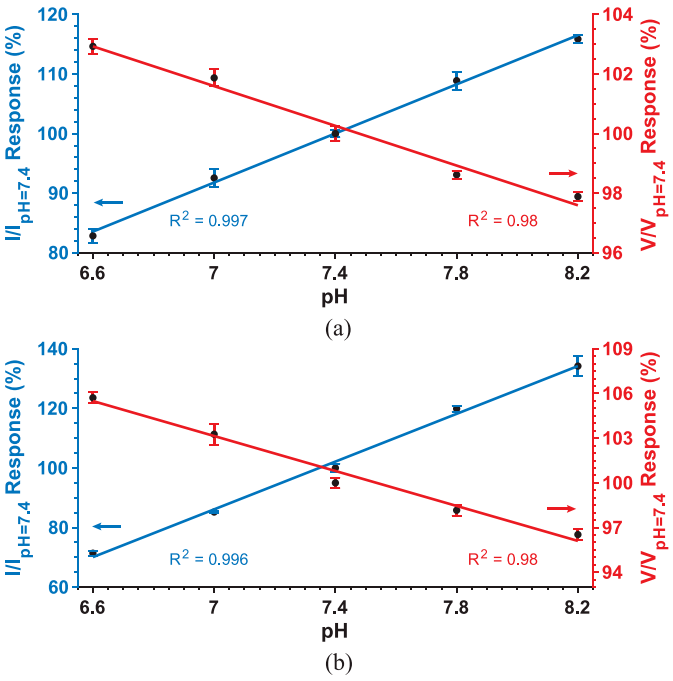

Fig. 11. Sensor performance vs. variation in solution pH for (a) fentanyl and (b) morphine, showing the normalized peak current (blue) and peak potential (red) responses ($n = 3$).

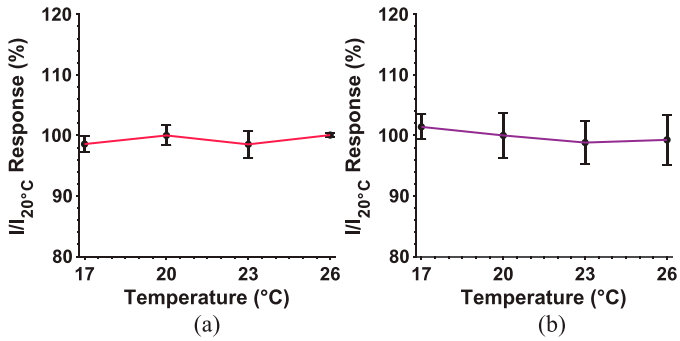

Fig. 12. Temperature stability of (a) fentanyl and (b) morphine sensors (pH 7.4) illustrating normalized changes in peak current responses ($n = 3$).

E. Effect of pH and Temperature

Electrolyte (buffer) pH and temperature commonly impact the performance of electrochemical sensors. To quantify their effects, fentanyl and morphine samples were measured across varying pH and temperature ranges that could be experienced in a hospital setting. In the case of IV opioid administration, standardized saline buffer solutions, which provide pH consistency, are utilized. Nevertheless, minor pH deviations would be expected in instances of solution tampering. Similarly, temperature is often well-regulated in hospitals to maintain drug efficacy, prevent the spread of disease, and ensure patient comfort. However, regional climate differences, the time of year, and the location in the hospital (operating room vs. patient room) could result in up to 5 °C fluctuations.

Voltammograms were measured for both opioids at 50 µg/mL concentrations with pH values ranging from 6.6 to 8.2, centered at 7.4. The recorded voltammograms exhibited shifts in peak currents and potential positions. These peak currents and potentials are plotted as a function of pH in Fig. 11(a) and 11(b) for fentanyl and morphine, respectively. With increasing pH, both sensors show an increase in peak current response and a linear decrease in oxidation potential. All data is normalized to the peaks and positions from the pH 7.4 measurement to display relative shifts from the nominal value. The results confirm that the oxidation response for fentanyl and morphine are pH dependent, as predicted by the Nernst equation, and are in line with prior work [31], [34], [39].

The temperature dependence was studied by measuring 50 µg/mL samples inside a temperature-controlled water bath (pH 7.4). The temperature was altered between 17 °C and 26 °C to cover a wider range than the expected hospital variation. Fig. 12 shows the resulting peak current deviation for fentanyl [see Fig. 12(a)] and morphine [see Fig. 12(b)], where the responses are normalized to the room temperature data (20 °C). The sensors remain insensitive to temperature as the mean responses stayed within 1.5% of the room temperature value for both opioids over the entire range. Additionally, no shifting in the peak potentials was observed for either opioid.

These data demonstrate that the sensors resist reasonably anticipated fluctuations in pH or temperature. Moreover, since the peak current and potential deviations are linear with pH, they can be corrected via standard linear calibration methods. If accurate opioid quantification is required, pre- and post-calibration should be performed on all measurements to account for the pH and, ideally, temperature.

F. Reproducibility

Due to imperfections in the fabrication process, it is expected that SPEs exhibit some degree of mismatch between sensors. To assess the reproducibility, 20 independent sensors were tested for both fentanyl and morphine. The first 10 electrodes were taken from one box of electrodes, while the final 10 electrodes were taken from a second box (randomly selected) to gain further statistical insight into local variation within a single box and the lot-to-lot variation. 50 µg/mL fentanyl and morphine samples were measured with each sensor. Fig. 13 displays the measured data normalized to the mean of the 20 samples (left), and the box and whisker plot (right) shows the same data. The variation is assessed by computing the relative standard deviation (RSD) for the individual boxes and the combined data. For fentanyl, the calculated RSDs were 6.15% for box 1 (slightly higher due to the identification of one outlier), 3.56% for box 2, and 5.52% for both boxes together. For morphine, the RSDs were 4.30% for box 1, 4.68% for box 2, and 4.40% combined. All responses (outlier excluded) fell within 10% of the mean for the respective opioids. Both sensors are highly reproducible and consistent, with no substantial difference observed between boxes.

G. Interference Studies

To firmly identify instances of solution tampering and diversion, the opioid sensor should be resilient to interfering compounds that may be present in a heterogeneous sample.

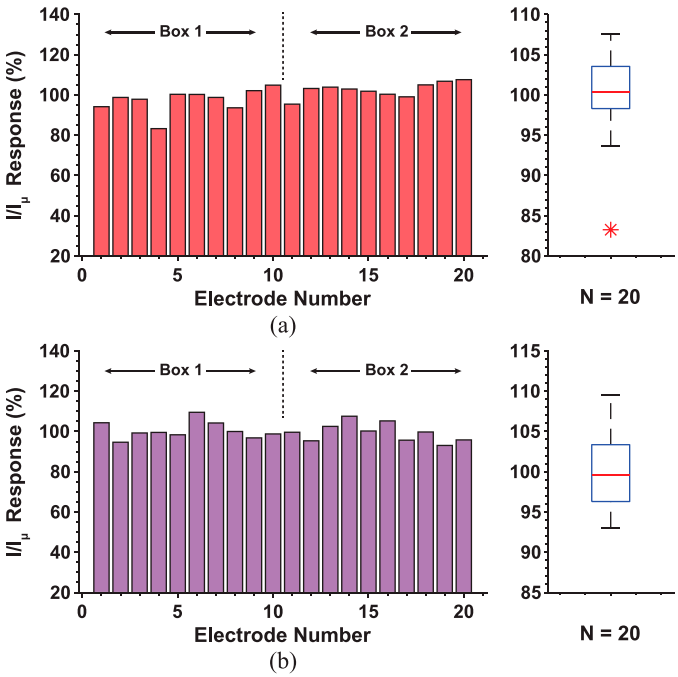

Fig. 13. Reproducibility of the (a) fentanyl and (b) morphine sensors across 20 SPE sensors from two different boxes. Peak current responses normalized to the sample mean (left) and corresponding box and whisker plots (right).

Although recent news articles reported instances of the medication being replaced altogether with saline or tap water, distinguishing the opioid from off-target compounds is still important. As such, the fentanyl and morphine sensor specificities were studied in mixtures containing common cutting agents and diluents such as glucose (Glu), fructose (Fru), sucrose (Suc), acetaminophen (AC), caffeine (CA), ascorbic acid (AA), and uric acid (UA). The voltammograms of these individual interferers are shown in Fig. 14, along with fentanyl and morphine, to demonstrate that their oxidation peaks (if any) do not overlap with the target opioid peaks.

Next, measurements were performed on samples containing 50 μg/mL fentanyl or morphine mixed with either 5 mM of the three sugar compounds or 100 μM of AC, CA, AA, and UA. The resulting interference study data is shown in Fig. 15, where the fentanyl (or morphine) peak current response in the presence of an interferer is expressed as a percent difference relative to the peak current in a pure 50 μg/mL sample containing only the target opioid. No oxidation peaks were observed for the sugars, resulting in no interference. No peaks for caffeine were observed within the scanned potential window since caffeine has an oxidation potential outside this range [56]. Ascorbic acid, uric acid, and acetaminophen all have a single oxidation peak at 230, 280, and 340 mV, respectively. When combined with fentanyl, these peaks remain far enough away from the fentanyl peak at 880 mV to limit their impact on the fentanyl response to a worst-case 8.9%. When mixed with morphine, these peaks are close to the first morphine peak at 340 mV; however, the second morphine peak remains largely unaffected by these interferers, similar to fentanyl, with uric acid presenting the largest signal deviation at 6.3%. While there are some signal changes, these are all within the

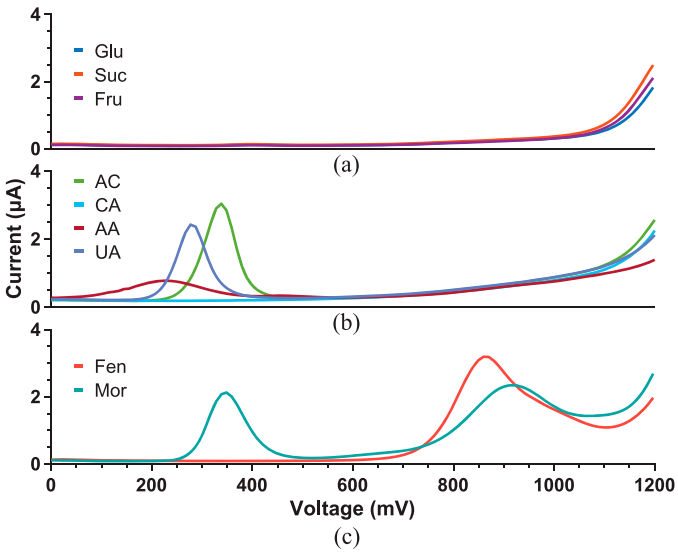

Fig. 14. Voltammograms of common interfering substances. Responses are separated between (a) sugar molecules and (b) the remaining substances. Fentanyl and morphine are shown in (c) as references.

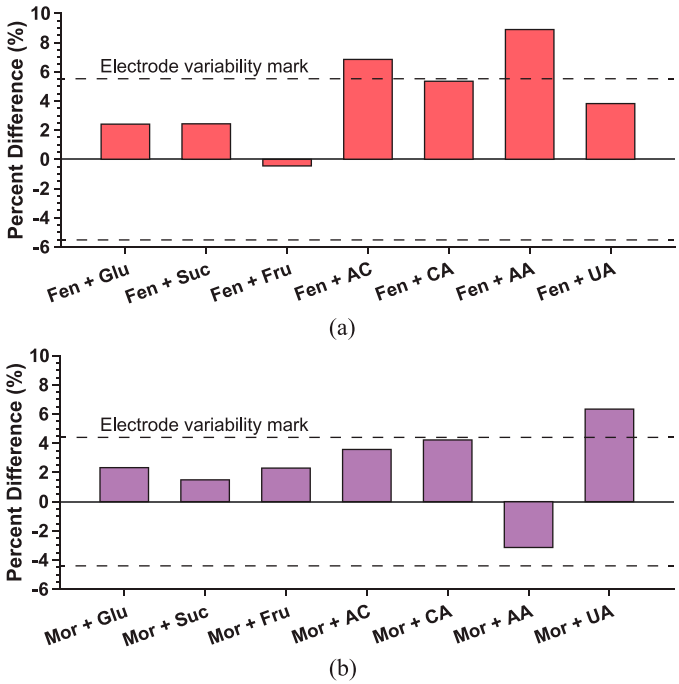

Fig. 15. Selectivity of the (a) fentanyl and (b) morphine to mixtures of common interfering agents. Data shows the target opioid response in the presence of an interferer relative to its response in a pure target sample. Dashed lines placed at the sensor RSD values from the reproducibility data.

sensor-sensor variability and are not statistically significant. In summary, both opioid sensors demonstrate <10% variation in the presence of strong interfering compounds, indicating that the sensors have good selectivity and can distinguish tampered solutions.

To assess a "worst-case" scenario that compounds the impacts of sensor reproducibility and interference, a solution containing fentanyl (or morphine) and all interferers (which were individually presented in Fig. 14) was prepared, and the responses were

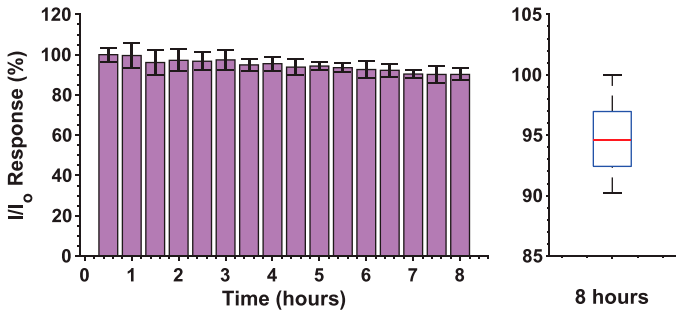

Fig. 16. Stability of the morphine sensor over 8 hours measured every 30 minutes ($n = 3$). Peak current response normalized to the starting value (left) and corresponding box and whisker plot (right).

measured across 8 different SPEs. The fentanyl sensor had a mean signal change of 14.46% with a standard deviation of 2.73%, while the morphine sensor had a 21.86% change in mean signal with a 1.26% standard deviation. Note that a malicious tampering scenario like this, although possible, is unlikely to occur as all reported tampering cases to date detail the doctor/nurse's intention to steal the opioid solution and not to prepare a dangerous cocktail of substances. However, it is critical to note that for this application, the primary objective is to identify an instance of opioid tampering. Since fentanyl and morphine exhibit distinct peak features (peak width, steepness, asymmetry, etc.), the mere presence of additional peaks (or lack thereof) or irregularities in the peak features will alert the staff that tampering has occurred. This allows the binary determination of whether the sample was tampered with to remain correct, even in scenarios of overlapping oxidation peaks (*e.g.*, the combination of fentanyl and morphine), simple mix-ups of patient solutions, or malicious substitutions. This was the principal motivation behind adopting a non-specific electrooxidation approach for this sensor, as it is intentionally desired to identify the presence of foreign substances.

H. Electrode Stability

Maintaining the stability of the electrochemical sensor is critical to ensuring that accurate measurements can be repeatedly taken throughout an entire surgical procedure. To study this effect, 50 µg/mL morphine samples were measured every 30 minutes for 8 hours using the same SPE. Morphine was utilized for this study since fentanyl is more commonly administered quickly via bolus dosage, whereas morphine administration can be prolonged for post-operation pain management. The stability results are displayed in Fig. 16, where the measured peak currents at each time point are normalized to the initial point. The sensor retains >90% of its initial response over the 8 hours, sufficient to cover most surgical procedures. Thus, the sensor can be replaced daily for continuous monitoring applications or any time the opioid is replaced to prevent cross-contamination.

I. Blind Study

A blind study was run to evaluate the proposed system's real-world performance. Contrived samples ($n = 20$) were created from various interferers with and without fentanyl. Each sample was assigned a random letter and then measured using the device (see Fig. 17). A binary classifier was written in Python (v3.12) using Keras (v3.2) and TensorFlow (v2.16) to identify the voltammograms as adultered or not adultered (*i.e.*, pure fentanyl in the range listed in Table I). The data from the previous studies was used to train the classifier; however, there were only 697 samples, so the dataset was augmented by adding white Gaussian noise ($\sigma = 0.1$ µA), shifting ($\Delta V = \pm 60$ mV), and scaling ($\pm 10\%$) the samples randomly. This process increased the dataset to 27,007 samples (85% adultered). Each voltammogram has 109 current measurements, which is too high dimensionality to use directly as the input to the neural network, given the limited dataset size. Instead, principal component analysis (PCA) was applied to reduce the dimensionality to 8 principal components that maintained 95% of the variance. The PCA output was then used to train a feedforward neural network (8 inputs followed by 2 hidden layers with 8 nodes each and a single output) with dropout regularization to prevent overfitting. On the training data, the classifier achieved 98% accuracy. The pipeline was then applied to the data collected in the blind study, and the results are shown in Table II, along with the true result after unblinding the samples. The predictions were all correct except for Sample F, which contained fentanyl (50 µg/mL) and ketamine (50 µg/mL). This outcome is obvious in hindsight since no samples in the training set had peaks near ketamine. The accuracy can likely be improved with additional data, but it is already quite good. It is worth pointing out that the classification pipeline was run on a computer but could be easily ported onto the microcontroller.

VI. Comparison to Prior Art

Table III compares this work to prior art electrochemical sensors for fentanyl and morphine detection, focusing on different opioid detection applications. Although there have been many works that seek to measure these opioids for overdose prevention and illicit substance identification [57], [58] (some of which achieve impressive LODs and dynamic ranges through elaborate modification steps), this work is the first to address the problem of opioid tampering in hospitals. This was accomplished through system-level integration of an opioid sensor (achieving sufficient LOD and dynamic range for this application), flow cell, and a miniaturized potentiostat. These features enable the system to be portable and battery-powered with wireless communication, which is lacking from many prior works that focus solely on the electrochemical sensor, hindering their adoption in clinical/forensic applications. It is also worth noting that electrochemical sensors for other types of illicit drugs of abuse, including cocaine, methamphetamine, and heroin, have also been reported but are not the focus of this comparison [59].

At the surface, the medication tampering solution presented herein may appear similar in objective to therapeutic drug monitoring or personalized dosing, where a patient's drug concentrations are measured *in vivo,* allowing doctors to make optimized dosage adjustments according to an individual's response. In this scenario, the works presented in [41], [42] are an attractive

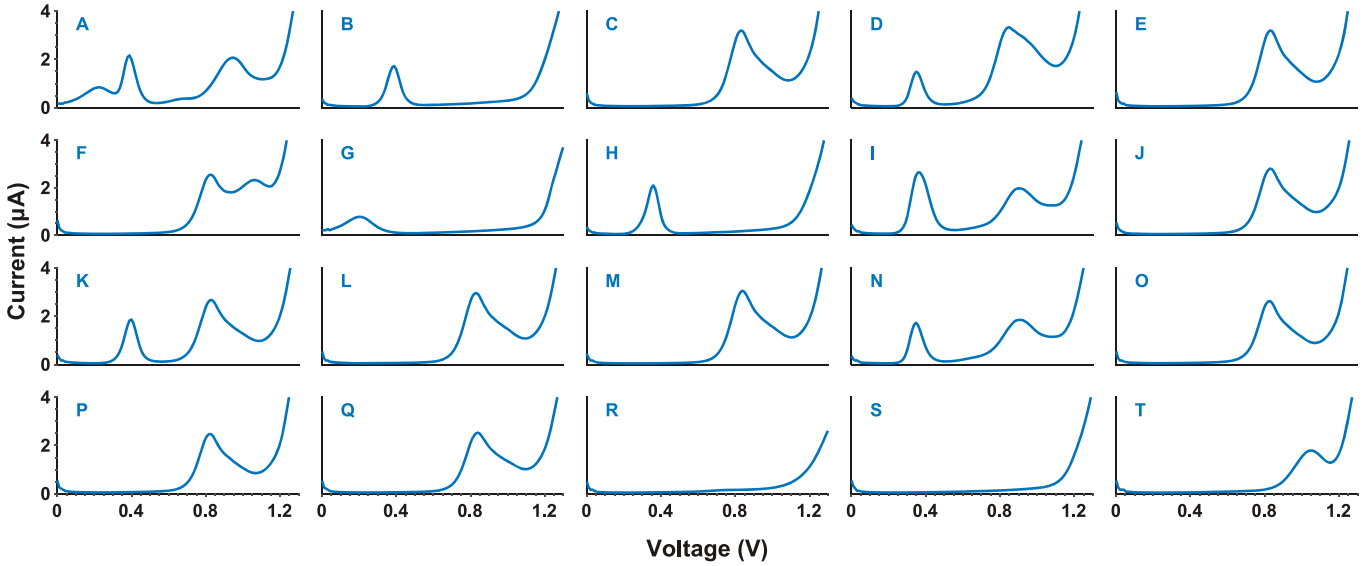

Fig. 17. Voltammogram responses of the contrived samples ($n = 20$) used in the blind fentanyl classification study.

solution. However, the tampering application is targeting something fundamentally different: if the opioid is detected solely *in vivo*, then there is nothing to prevent the patient from metabolizing a potentially dangerous substance. As such, this work explicitly targets opioid sensing before administration.

VII. Concluding Remarks

This work reports the design and validation of an electrochemical-based opioid monitoring system. Through the development of a miniaturized potentiostat, flow cell, and accompanying sensors for fentanyl and morphine, we enable the real-time quantification of intravenous opioid medication to combat solution tampering and diversion. The hardware components are battery-operated, BLE compatible, and ultra-low power, consuming just 36 μA in the sleep mode and providing >30 days of battery lifetime with a 10-minute sampling interval. The electrooxidation sensing scheme leverages screen-printed electrodes and differential pulse voltammetry to achieve sensitive opioid detection, with a limit of detection of 1.26 and 2.75 μg/mL for fentanyl and morphine, respectively. Real-time measurements connected to a flow cell and IV tubing were demonstrated, illustrating the system's suitability for direct integration into hospital IV setups. The reported sensors remain resilient to pH, temperature, and potential interfering substances while maintaining strong reproducibility and stability. With a machine-learning classifier, this electrochemical detection approach demonstrated rapid and automatic identification of tampered opioid solutions with high accuracy.

Ultimately, we hope that this system helps close the loop in opioid administration, allowing doctors to make timely intervention in instances of incorrect medication dosage. The authors would like to stress that opioid tampering in hospitals is a rare occurrence, as the vast majority of doctors/nurses work diligently to prevent these scenarios. The intent of the reported system is to work in tandem with hospital workers to improve patient outcomes, rather than to scrutinize or inflict blame upon them for otherwise infrequent mistakes. Future work on this topic will focus on directly integrating pH and temperature sensors into the hardware/sensor so that real-time calibration can occur. Importantly, this work targeted fentanyl and morphine; however, many other drugs possess an electrochemical signature that could be detected. This device could also be used with an electronic drug delivery system, enabling automated feedback control and personalized medication.

TABLE II
Classification Results of the Fentanyl Sample Blind Study

Sample	Contents	Prediction	True
A	Ascorbic Acid + Morphine	Adultered	Adultered
B	Glucose + Diazepam + Acetaminophen	Adultered	Adultered
C	Fentanyl	Not adultered	Not adultered
D	Fentanyl + Morphine	Adultered	Adultered
E	Fentanyl	Not adultered	Not adultered
F	Ketamine + Fentanyl	**Not Adultered**	**Adultered**
G	Ascorbic Acid	Adultered	Adultered
H	Acetaminophen	Adultered	Adultered
I	Acetaminophen + Morphine	Adultered	Adultered
J	Fentanyl	Not adultered	Not adultered
K	Acetaminophen + Fentanyl	Adultered	Adultered
L	Fentanyl	Not adultered	Not adultered
M	Fentanyl	Not adultered	Not adultered
N	Morphine	Adultered	Adultered
O	Fentanyl	Not adultered	Not adultered
P	Fentanyl	Not adultered	Not adultered
Q	Fentanyl	Not adultered	Not adultered
R	Tap Water	Adultered	Adultered
S	1× PBS	Adultered	Adultered
T	Ketamine	Adultered	Adultered

TABLE III
COMPARISON TO PRIOR ART FENTANYL AND MORPHINE SENSORS

Application/Form Factor	Target Drug(s)	Electrode	Method	LoD [µM]	DR [µM]	Portable Reader?	Ref.
Illicit drug identification Wearable glove	Fentanyl	SPCE–RTIL/MWCNT	SWV	10	10 – 100	Commercial Emstat3	[30]
Opioid overdosing Microneedle array	Fentanyl	F1: CP F2: CP–CNT/Au/RGO/PVC	SWV	F1: 10 F2: 0.05	F1: 10 – 200 F2: 0.05 – 0.3	Commercial Emstat3	[41]
Anesthetic drug dosing Surgical microcatheter	Fentanyl	F1: CP–CNT/PVC F2: CP–CNT/Au/erGO/PVC	SWV	F1: 5 F2: 0.0022	F1: 5 – 50 F2: 0.003 – 0.024	Commercial Emstat3	[42]
Analgesic drug detection Sensor electrode	Fentanyl	GCE–NiO/CNT	DPV	0.01	10 – 160	None	[57]
Illicit drug identification Disposable strip	Fentanyl	SPCE (laser-induced carbon)	SWV	1	20 – 200	Commercial Sensit BT	[40]
Abusive drug identification Sensor electrode	Morphine	CPE–Zn_2SnO_4/GO	DPV	0.011	0.02 – 15	None	[34]
Abusive drug identification Sensor electrode	Morphine	CPE–M-CNFs	DPV	0.0019	0.0033 – 245	None	[36]
Post-operative pain control Sensor electrode	Morphine	SWCNT/Nafion	DPV	0.071	0.05 – 10	None	[58]
Opioid tampering Hospital IV monitor	**Fentanyl Morphine**	**SPCE (commercial)**	**DPV**	**F: 3.7 M: 9.6**	**F: 14.9 – 297.2 M: 17.5 – 350.4**	**Custom AD5940**	**This Work**

IV: intravenous
CNT: carbon nanotube
GO: graphene oxide
CP: carbon paste
DR: dynamic range
SPCE: screen-printed carbon electrode
RTIL: room temperature ionic liquid
MWCNT: multi-walled carbon nanotube
GO: electrochemically reduced graphene oxide
SWCNT: single-walled carbon nanotubes
CPE: carbon paste electrode
PVC: polyvinyl chloride
LoD: limit of detection
GCE: glassy carbon electrode
M-CNFs: magnetic carbon nanofibers
DPV: differential pulse voltammetry
SWV: square wave voltammetry
RGO: reduced graphene oxide

REFERENCES

[1] C. F. Ramos-Matos, K. G. Bistas, and W. Lopez-Ojeda, "Fentanyl," in *StatPearls*, Treasure Island, FL, USA: StatPearls Publishing, 2023, Accessed: May 1, 2023. [Online]. Available: http://www.ncbi.nlm.nih.gov/books/NBK459275/

[2] P. B. Murphy, S. Bechmann, and M. J. Barrett, "Morphine," in *StatPearls*, Treasure Island, FL, USA: StatPearls Publishing, 2023, Accessed: May 29, 2023. [Online]. Available: http://www.ncbi.nlm.nih.gov/books/NBK526115/

[3] "Opioids." Johns Hopkins Medicine. Accessed: Feb. 11, 2024. [Online]. Available: https://www.hopkinsmedicine.org/health/treatment-tests-and-therapies/opioids

[4] "Understanding the opioid overdose epidemic." CDC. Accessed: Feb. 11, 2024. [Online]. Available: https://www.cdc.gov/opioids/basics/epidemic.html

[5] J. Marnin, "Nurse caught stealing fentanyl from critical care patient's IV bag in hospital, feds say." Miami Herald. Accessed: May 1, 2023. [Online]. Available: https://www.miamiherald.com/news/nation-world/national/article272561207.html

[6] "District of Kansas | Former Health Care Worker Sentenced for Fentanyl Thefts." United States Department of Justice. Accessed: Jun. 13, 2023. [Online]. Available: https://www.justice.gov/usao-ks/pr/former-health-care-worker-sentenced-fentanyl-thefts

[7] G. Moran, "He says he woke up during surgery. Lawsuit blames it on fentanyl use by anesthesiologist." San Diego Union-Tribune. Accessed: Jun. 13, 2023. [Online]. Available: https://www.sandiegouniontribune.com/news/courts/story/2022-11-25/fentanyl-addiction-lawsuit-hay-ucsd

[8] "District of Massachusetts | Berkley Nurse Sentenced for Tampering with Patients' Fentanyl." United States Department of Justice. Accessed: Jun. 14, 2023. [Online]. Available: https://www.justice.gov/usao-ma/pr/berkley-nurse-sentenced-tampering-patients-fentanyl

[9] O. of R. Affairs, "Supervisory paramedic sentenced to three years in federal prison for stealing fentanyl and tampering with drugs intended for patients," FDA, May 2023. Accessed: Jun. 14, 2023. [Online]. Available: https://www.fda.gov/inspections-compliance-enforcement-and-criminal-investigations/press-releases/supervisory-paramedic-sentenced-three-years-federal-prison-stealing-fentanyl-and-tampering-drugs

[10] I. Wright, "ICU nurse steals fentanyl IV bags and swaps fluid with unknown liquid, Florida cops say." Miami Herald. Accessed: Feb. 11, 2024. [Online]. Available: https://www.miamiherald.com/news/state/florida/article283410383.html

[11] "Janesville ex-nurse gets 15 months prison for fentanyl theft." Accessed: Feb. 11, 2024. [Online]. Available: https://madison.com/news/local/crime-courts/fentanyl-theft-nurse-janesville-hospital-prison/article_0a373e56-53cd-11ee-93a7-d3c076e2ec37.html

[12] K. H. Berge, K. R. Dillon, K. M. Sikkink, T. K. Taylor, and W. L. Lanier, "Diversion of drugs within health care facilities, a multiple-victim crime: Patterns of diversion, scope, consequences, detection, and prevention," *Mayo Clin. Proc.*, vol. 87, no. 7, pp. 674–682, Jul. 2012, doi: 10.1016/j.mayocp.2012.03.013.

[13] W. Ling, L. Mooney, and M. Hillhouse, "Prescription opioid abuse, pain and addiction: Clinical issues and implications," *Drug Alcohol Rev.*, vol. 30, no. 3, pp. 300–305, 2011, doi: 10.1111/j.1465-3362.2010.00271.x.

[14] M. Osburn, "ONLY ON NBC5: Sources say 8-9 died at RRMC from drug diversion." KOBI-TV NBC5/KOTI-TV NBC2. Accessed: Feb. 11, 2024. [Online]. Available: https://kobi5.com/news/crime-news/only-on-5-sources-say-8-9-died-at-rrmc-from-drug-diversion-219561/

[15] P. M. Herout and B. L. Erstad, "Medication errors involving continuously infused medications in a surgical intensive care unit," *Crit. Care Med.*, vol. 32, no. 2, pp. 428, Feb. 2004, doi: 10.1097/01.CCM.0000108876.12846.B7.

[16] K. Kuck, L. Lofgren, and C. Lybbert, "Anesthesia patient monitoring 2050," *Anesthesia & Analgesia*, vol. 138, no. 2, Feb. 2024, Art. no. 273, doi: 10.1213/ANE.0000000000006660.

[17] G. Yu, F.-Q. Zhang, S.-E. Tang, M.-J. Lai, R.-B. Su, and Z.-H. Gong, "Continuous infusion versus intermittent bolus dosing of morphine: A comparison of analgesia, tolerance, and subsequent voluntary morphine intake," *J. Psychiatr. Res.*, vol. 59, pp. 161–166, Dec. 2014, doi: 10.1016/j.jpsychires.2014.08.009.

[18] T. Hack, J. Bisarra, S. Chung, and D. A. Hall, "Ensuring pain medication dosage: A real-time intravenous opioid monitoring system," in *Proc. 2023 IEEE Biomed. Circuits and Syst. Conf. (BioCAS)*, Oct. 2023, pp. 1–5, doi: 10.1109/BioCAS58349.2023.10388932.

[19] H. H. Maurer, "Advances in analytical toxicology: The current role of liquid chromatography–Mass spectrometry in drug quantification in blood and oral fluid," *Anal. Bioanal. Chem.*, vol. 381, no. 1, pp. 110–118, Jan. 2005, doi: 10.1007/s00216-004-2774-z.

[20] L. Harper, J. Powell, and E. M. Pijl, "An overview of forensic drug testing methods and their suitability for harm reduction point-of-care services," *Harm Reduction J.*, vol. 14, no. 1, Jul. 2017, Article no. 52, doi: 10.1186/s12954-017-0179-5.

[21] A. Haddad, M. A. Comanescu, O. Green, T. A. Kubic, and J. R. Lombardi, "Detection and quantitation of trace fentanyl in heroin by surface-enhanced Raman spectroscopy," *Anal. Chem.*, vol. 90, no. 21, pp. 12678–12685, Nov. 2018, doi: 10.1021/acs.analchem.8b02909.

[22] R. L. Stiller, A. M. Scierka, P. J. Davis, and D. Ryan Cook, "A brief technical communication: Detection of fentanyl in urine," *Forensic Sci. Int.*, vol. 44, no. 1, pp. 1–6, Jan. 1990, doi: 10.1016/0379-0738(90)90160-Z.

[23] G. Wang et al., "Development of a homogeneous immunoassay for the detection of fentanyl in urine," *Forensic Sci. Int.*, vol. 206, no. 1, pp. 127–131, Mar. 2011, doi: 10.1016/j.forsciint.2010.07.022.

[24] O. A. Farghaly, R. S. A. Hameed, and A.-A. H. Abu-Nawwas, "Analytical application using modern electrochemical techniques," *Int. J. Electrochem. Sci.*, vol. 9, no. 6, pp. 3287–3318, Jun. 2014, doi: 10.1016/S1452-3981(23)08010-0.

[25] A. C. Sun, C. Yao, A. G. Venkatesh, and D. A. Hall, "An efficient power harvesting mobile phone-based electrochemical biosensor for point-of-care health monitoring," *Sens. Actuators B: Chem.*, vol. 235, pp. 126–135, Nov. 2016, doi: 10.1016/j.snb.2016.05.010.

[26] A. Sun, A. G. Venkatesh, and D. A. Hall, "A multi-technique reconfigurable electrochemical biosensor: Enabling personal health monitoring in mobile devices," *IEEE Trans. Biomed. Circuits Syst.*, vol. 10, no. 5, pp. 945–954, Oct. 2016, doi: 10.1109/TBCAS.2016.2586504.

[27] H. Jiang, X. Zhou, S. Kulkarni, M. Uranian, R. Seenivasan, and D. A. Hall, "A Sub-1 μW multiparameter injectable BioMote for continuous alcohol monitoring," in *Proc. IEEE Custom Integr. Circuits Conf. (CICC)*, Apr. 2018, pp. 1–4, doi: 10.1109/CICC.2018.8357045.

[28] A. M. Arjun, P. H. Krishna, A. R. Nath, and P. A. Rasheed, "A review on advances in the development of electrochemical sensors for the detection of anesthetic drugs," *Anal. Methods*, vol. 14, no. 41, pp. 4040–4052, Oct. 2022, doi: 10.1039/D2AY01290A.

[29] S. A. Goodchild et al., "Ionic liquid-modified disposable electrochemical sensor strip for analysis of fentanyl," *Anal. Chem.*, vol. 91, no. 5, pp. 3747–3753, Mar. 2019, doi: 10.1021/acs.analchem.9b00176.

[30] A. Barfidokht et al., "Wearable electrochemical glove-based sensor for rapid and on-site detection of fentanyl," *Sensors Actuators B: Chem.*, vol. 296, Oct. 2019, Art. no. 126422, doi: 10.1016/j.snb.2019.04.053.

[31] E. Naghian, E. M. Khosrowshahi, E. Sohouli, F. Ahmadi, M. Rahimi-Nasrabadi, and V. Safarifard, "A new electrochemical sensor for the detection of fentanyl lethal drug by a screen-printed carbon electrode modified with the open-ended channels of Zn(II)-MOF," *New J. Chem.*, vol. 44, no. 22, pp. 9271–9277, Jun. 2020, doi: 10.1039/D0NJ01322F.

[32] E. Sohouli et al., "A glassy carbon electrode modified with carbon nanoonions for electrochemical determination of fentanyl," *Mater. Sci. Eng.: C*, vol. 110, May 2020, Art. no. 110684, doi: 10.1016/j.msec.2020.110684.

[33] P. Abraham, R. S. P. Vijayan, N. V. K. Sreevalsan, and V. Anithakumary, "Review—Review on the progress in electrochemical detection of morphine based on different modified electrodes," *J. Electrochem. Soc.*, vol. 167, no. 3, Feb. 2020, Art. no. 037559, doi: 10.1149/1945-7111/ab6cf6.

[34] H. Bagheri, H. Khoshsafar, A. Afkhami, and S. Amidi, "Sensitive and simple simultaneous determination of morphine and codeine using a Zn2SnO4 nanoparticle/graphene composite modified electrochemical sensor," *New J. Chem.*, vol. 40, no. 8, pp. 7102–7112, Aug. 2016, doi: 10.1039/C6NJ00505E.

[35] Y.-P. Hong, J.-M. Hu, J.-Q. Zhang, and C.-N. Cao, "Enhanced electrocatalytic activity for morphine oxidation at 2-aminoethanethiol self-assembled monolayer (SAM)-modified gold electrode," *Electrocatalysis*, vol. 4, no. 4, pp. 302–305, Dec. 2013, doi: 10.1007/s12678-013-0160-3.

[36] G. Bahrami, H. Ehzari, S. Mirzabeigy, B. Mohammadi, and E. Arkan, "Fabrication of a sensitive electrochemical sensor based on electrospun magnetic nanofibers for morphine analysis in biological samples," *Mater. Sci. Eng.: C*, vol. 106, Jan. 2020, Art. no. 110183, doi: 10.1016/j.msec.2019.110183.

[37] C. G. Bauer et al., "New enzyme sensors for morphine and codeine based on morphine dehydrogenase and laccase," *Fresenius J. Anal. Chem.*, vol. 364, no. 1, pp. 179–183, May 1999, doi: 10.1007/s002160051320.

[38] C. E. Ott, H. Cunha-Silva, S. L. Kuberski, J. A. Cox, M. J. Arcos-Martínez, and L. E. Arroyo-Mora, "Electrochemical detection of fentanyl with screen-printed carbon electrodes using square-wave adsorptive stripping voltammetry for forensic applications," *J. Electroanalytical Chem.*, vol. 873, Sep. 2020, Art. no. 114425, doi: 10.1016/j.jelechem.2020.114425.

[39] N. Wester et al., "Single-walled carbon nanotube network electrodes for the detection of fentanyl citrate," *ACS Appl. Nano Mater.*, vol. 3, no. 2, pp. 1203–1212, Feb. 2020, doi: 10.1021/acsanm.9b01951.

[40] R. K. Mishra, A. Krishnakumar, A. Zareei, U. Heredia-Rivera, and R. Rahimi, "Electrochemical sensor for rapid detection of fentanyl using laser-induced porous carbon-electrodes," *Microchim Acta*, vol. 189, no. 5, Apr. 2022, Art. no. 198, doi: 10.1007/s00604-022-05299-1.

[41] R. K. Mishra et al., "Continuous opioid monitoring along with nerve agents on a wearable microneedle sensor array," *J. Am. Chem. Soc*, vol. 142, no. 13, pp. 5991–5995, Apr. 2020, doi: 10.1021/jacs.0c01883.

[42] C. Moonla et al., "An integrated microcatheter-based dual-analyte sensor system for simultaneous, real-time measurement of propofol and fentanyl," *Talanta*, vol. 218, Oct. 2020, Art. no. 121205, doi: 10.1016/j.talanta.2020.121205.

[43] M. W. Glasscott, K. J. Vannoy, P. U. A. Iresh Fernando, G. K. Kosgei, L. C. Moores, and J. E. Dick, "Electrochemical sensors for the detection of fentanyl and its analogs: Foundations and recent advances," *TrAC Trends Analytical Chem.*, vol. 132, Nov. 2020, Art. no. 116037, doi: 10.1016/j.trac.2020.116037.

[44] Y. Qiu, Y. Tang, B. Li, and M. He, "Rapid detection of cocaine using aptamer-based biosensor on an evanescent wave fibre platform," *Roy. Soc. Open Sci.*, vol. 5, no. 10, Oct. 2018, Art. no. 180821, doi: 10.1098/rsos.180821.

[45] Y. Wu et al., "Microneedle aptamer-based sensors for continuous, real-time therapeutic drug monitoring," *Analytical Chem.*, vol. 94, no. 23, pp. 8335–8345, Jun. 2022, doi: 10.1021/acs.analchem.2c00829.

[46] C. Martin and C. Grgicak, "The effect of repeated activation on screen-printed carbon electrode cards," *ECS Trans.*, vol. 61, no. 26, Sep. 2014, Art. no. 1, doi: 10.1149/06126.0001ecst.

[47] B. J. Venton and D. J. DiScenza, "Chapter 3 - Voltammetry," in *Electrochemistry for Bioanalysis*, B. Patel, Ed., Amsterdam, Netherlands: Elsevier, 2020, pp. 27–50, doi: 10.1016/B978-0-12-821203-5.00004-X.

[48] W. Gao et al., "Fully integrated wearable sensor arrays for multiplexed in situ perspiration analysis," *Nature*, vol. 529, Jan. 2016, Art. no. 7587, doi: 10.1038/nature16521.

[49] A. Ainla et al., "Open-source potentiostat for wireless electrochemical detection with smartphones," *Anal. Chem.*, vol. 90, no. 10, pp. 6240–6246, May 2018, doi: 10.1021/acs.analchem.8b00850.

[50] H. Yu et al., "The effect of dilution and prolonged injection time on fentanyl-induced coughing," *Anaesthesia*, vol. 62, no. 9, pp. 919–922, Aug. 2007, doi: 10.1111/j.1365-2044.2007.05147.x.

[51] T. Deaton, J. D. Auten, and M. A. Darracq, "Nebulized fentanyl vs intravenous morphine for ED patients with acute abdominal pain: A randomized double-blinded, placebo-controlled clinical trial," *Amer. J. Emergency Med.*, vol. 33, no. 6, pp. 791–795, Jun. 2015, doi: 10.1016/j.ajem.2015.03.046.

[52] "DEA Issues Nationwide Alert on Fentanyl as Threat to Health and Public Safety." Accessed: Jun. 13, 2023. [Online]. Available: https://www.dea.gov/press-releases/2015/03/18/dea-issues-nationwide-alert-fentanyl-threat-health-and-public-safety

[53] A. Shrivastava, "Methods for the determination of limit of detection and limit of quantitation of the analytical methods," *Chronicles Young Sci.*, vol. 2, pp. 21–25, Jun. 2011, doi: 10.4103/2229-5186.79345.

[54] G. L. Holmquist, "Opioid metabolism and effects of cytochrome P450," *Pain Med.*, vol. 10, no. suppl_1, pp. S20–S29, Apr. 2009, doi: 10.1111/j.1526-4637.2009.00596.x.

[55] H. S. Smith, "Opioid metabolism," *Mayo Clinic Proc.*, vol. 84, no. 7, pp. 613–624, Jul. 2009, doi: 10.4065/84.7.613.

[56] K. Y. Tajeu, E. Ymele, S. L. Zambou Jiokeng, and I. K. Tonle, "Electrochemical sensor for caffeine based on a glassy carbon electrode modified with an Attapulgite/Nafion Film," *Electroanalysis*, vol. 31, no. 2, pp. 350–356, 2019, doi: 10.1002/elan.201800621.

[57] H. Ding and W. Tao, "Synthesis of NiO-CNTs nanocomposite for modification of glassy carbon electrode and application for electrochemical determination of fentanyl as an opioid analgesic drug," *Int. J. Electrochem. Sci.*, vol. 16, no. 11, Nov. 2021, Art. no. 211137, doi: 10.20964/2021.11.33.

[58] N. Wester et al., "Simultaneous detection of morphine and codeine in the presence of ascorbic acid and uric acid and in human plasma at nafion single-walled carbon nanotube thin-film electrode," *ACS Omega*, vol. 4, no. 18, pp. 17726–17734, Oct. 2019, doi: 10.1021/acsomega.9b02147.

[59] Z. Dai, "Recent advances in the development of portable electrochemical sensors for controlled substances," *Sensors*, vol. 23, Jan. 2023, Art. no. 6, doi: 10.3390/s23063140.

Tyler Hack (Student Member, IEEE) received the B.S. degree in electrical engineering from Santa Clara University (SCU), CA, USA, in 2019 and the M.S. degree in electrical and computer engineering from the University of California San Diego (UCSD), San Diego, CA, USA, in 2021, where he is currently working toward the Ph.D. degree. He has held internship positions at Vishay Siliconix, Santa Clara, CA, USA, and Maxim Integrated, Santa Clara, CA, USA, where he worked on integrated power converters and low-power analog circuit design. His research interests include biomedical analog circuits and systems for wearable devices toward continuous health monitoring, sensor interfaces, and low-power RF circuit design.

Joel Bisarra (Student Member, IEEE) received the B.S. and M.S. degrees in electrical and computer engineering from the University of California San Diego (UCSD), San Diego, CA, USA, in 2022 and 2023, respectively. He is currently holding an internship position at pSemi, San Diego, CA, USA, where he worked on RF switch and LNA design and characterization. He has also held an internship position at Medtronic, Los Angeles, CA, USA, where he worked on board-level design of test interfaces for biomedical sensors.

Saeromi Chung received the B.S., M.S., and Ph.D. degrees in chemistry from Pusan National University, South Korea, in 2010, 2012, and 2019, respectively. From 2019 to 2023, she then conducted research as a Postdoctoral Scholar with the Department of Electrical and Computer Engineering, University of California San Diego (UCSD), specializing in developing electrochemical biosensors utilizing DNA, proteins, and nanomaterials. She expanded this expertise during her time at Persperion Diagnostics. Her research interests include leveraging electrochemical sensors for point-of-care study.

Shekher Kummari received the M.Sc. degree from the University College of Science, Osmania University, Hyderabad, Telangana, India, in 2013, and the Ph.D. degree in chemistry from the Department of Chemistry, National Institute of Technology Warangal (NITW), in 2021. He worked as a Postdoctoral Scholar for one year on the development of strip-based sensors for on-site detection of organophosphate nerve agents and illicit drugs with the Indian Institute of Technology Palakkad (IIT – Palakkad), Palakkad, Kerala, India. Currently, he is a Postdoctoral Fellow with the University of California San Diego (UCSD), San Diago, CA, USA. His research interests include developing nanomaterial-based electrochemical biosensors for point-of-care/point-of-use biomarker detection.

Drew A. Hall (Senior Member, IEEE) received the B.S. degree in computer engineering with honors from the University of Nevada, Las Vegas, NV, USA, in 2005, and the M.S. and Ph.D. degrees in electrical engineering from Stanford University, Stanford, CA, USA, in 2008 and 2012, respectively. From 2011 to 2013, he was a Research Scientist with the Integrated Biosensors Laboratory at Intel Corporation, Santa Clara, CA, USA. Since 2013, he has been with the Department of Electrical and Computer Engineering, University of California San Diego, where he is currently a Full Professor. His research interests include bioelectronics, biosensors, analog circuit design, medical electronics, and sensor interfaces. He won first place in the inaugural international IEEE Change the World Competition and first place in the BME-IDEA invention competition, both in 2009. He received the Analog Devices Outstanding Designer Award in 2011, an Undergraduate Teaching Award in 2014, the Hellman Fellowship Award in 2014, an NSF CAREER Award in 2015, and an NIH Trailblazer Award in 2019. He is also a Tau Beta Pi Fellow. He has served as an Associate Editor of the IEEE TRANSACTIONS ON BIOMEDICAL INTEGRATED CIRCUITS since 2015, a Member of the CICC Technical Program Committee since 2017, a Member of the ISSCC Technical Program Committee since 2020, and an Associate Editor of the IEEE SOLID-STATE CIRCUITS LETTERS since 2021.